

## Observation of Moving Dislocation Kinks and Unpinning

H. R. Kolar,<sup>1</sup> J. C. H. Spence,<sup>1,\*</sup> and H. Alexander<sup>2</sup>

<sup>1</sup>*Department of Physics and SEM, Arizona State University, Tempe, Arizona 85287*

<sup>2</sup>*Universitat zu Koln, Abteilung Fur Metallphysik im II Physikalischen Institut, Zulpicher Strasse 77, D 50937 Koln, Germany*  
(Received 15 May 1996)

Atomic resolution electron microscopy has been used to obtain images of moving dislocation kinks on partial dislocations at 600 °C in silicon. Video difference images are used to obtain direct estimates of kink velocity. Observations of kink delay at obstacles, thought to be oxygen atoms at the dislocation core, yield unpinning energies and parameters of the obstacle theory of kink motion. The kink formation energy is obtained from the distribution of kink pair separations in low-dose images and is compared to the kink migration energy. Unlike metals, kink migration rather than formation controls the velocity of unobstructed dislocations in silicon under these experimental conditions. [S0031-9007(96)01391-9]

PACS numbers: 61.72.Lk, 62.20.Fe, 73.61.Cw

It has been known for many years that the strength of ductile material is controlled by the motion of dislocations on the most densely packed glide planes of a crystal. Dislocation motion results if thermal fluctuations throw a segment of line forward, generating kink pairs, which are driven apart along the line by the application of an external stress. In silicon, the low energy Peierls valleys and dislocations run along  $\langle 110 \rangle$ , dislocations are dissociated, and kinks are narrow due to the high Peierls stress [Fig. 1(a)]. Because of this high stress, unlike metals, semiconductors become ductile only at an appreciable fraction of their melting point. Thus the fundamental atomic processes which control the mechanical properties of ductile matter are double kink nucleation and stress-assisted growth along a secondary Peierls potential. Evidence for the existence of kinks (from techniques such as pulse deformation, internal friction, weak-beam electron microscopy, and spectroscopy) is indirect and it remains uncertain whether the double kink nucleation free energy  $2F_k$ , the migration free energy  $W_m$ , or kink obstacles control dislocation motion in semiconductors. In this Letter we address these questions using atomic resolution transmission electron microscopy (TEM) and present the first images of moving and stationary dislocation kinks, from which we obtain values of the kink formation, mobility, and unpinning energies.

The most successful theory of dislocation motion [1] considers the nucleation of double kinks (with separation  $x$ ) and their diffusion and drift under an external stress  $\sigma$  by one-dimensional analogy with classical steady-state nucleation theory for particles of size  $x$ . Then the equilibrium distribution of kink separations (constrained to zero kink current) per unit length of line is

$$c_c(x) = a^{-2} \exp[-F(x)/kT], \quad (1)$$

with dimensions  $L^{-2}$  [1]. Here  $a$  is the reconstructed period along the line, and the free energy of kink-pair formation in the presence of the large stresses used in our experiments is [2]

$$F(x) = 2F_k - \mu b^2 h^2 / 8\pi x - \sigma b h x, \quad (2)$$

where  $h$  is the kink height and  $\mu$  the shear modulus. The second term represents the attractive kink-kink strain interaction (tending to annihilate by recombination kink pair embryos less than the critical separation  $x^*$ ) while the last term describes the external stress which drives kinks apart. The kink velocity for a dislocation with Burgers vector  $b$  is

$$v_k = \frac{\sigma b h v_D a^2}{kT} \exp(-W_m/kT) = \frac{\sigma b h}{2kT} D_p, \quad (3)$$

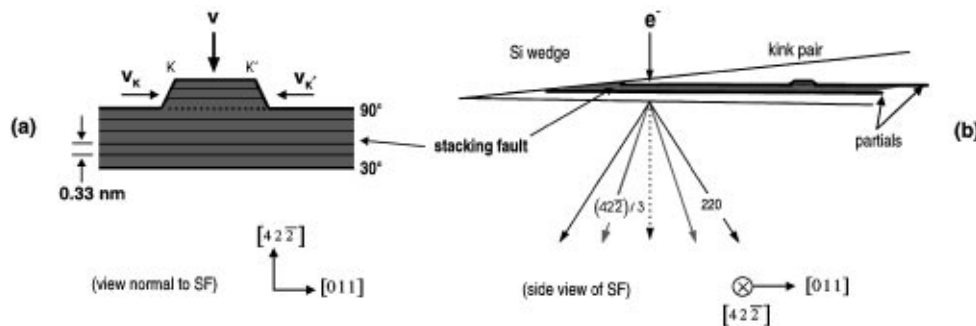


FIG. 1. (a) Experimental geometry. Stacking fault on  $(\bar{1}\bar{1})$  separating  $30^\circ$  and  $90^\circ$  partial dislocation lines, with Peierls valleys along  $[011]$  and kink pair  $K, K'$  shown. By running together (as in Fig. 2) these kinks advance the dislocation line in direction  $V$ , resulting in the elimination of the “bulge” in the  $90^\circ$  segment. (In Fig. 3 they run apart.) (b) Side view, along  $[42\bar{2}]$ , indicating “forbidden” beams generated by SF and bulk  $(220)$  beams. Shaded strip is normal to beam.

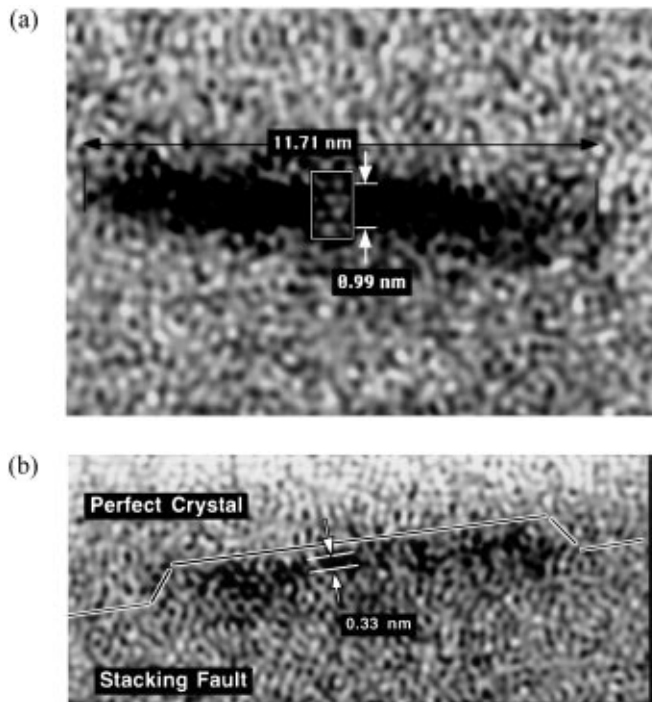


FIG. 2. (a) Difference between filtered video images of a moving  $90^\circ$  partial dislocation in silicon at  $600^\circ\text{C}$ , viewed along  $[111]$ . Dark strip is SF three Peierls valleys wide ( $0.99\text{ nm}$ ), eliminated by passage of several kinks. Inset shows experimental SF image for scale. (b) Similar for  $90^\circ$  partial segment, one Peierls valley wide.

where  $\nu_D$  is the Debye frequency ( $1.3 \times 10^{13}\text{ sec}^{-1}$ ),  $D_p$  the double kink diffusion coefficient, and  $W_m = U_m - TS_m$  the free energy of kink migration (similarly  $F_k = U_k - TS_k$ ). Theoreticians compute internal energies  $U_m$  (the sum of elastic and core energies); experiments measure either  $W_m$  or  $U_m$ . Our  $U_m$  values assume [3]  $S_k(90^\circ) = 0.5k$  and  $S_m(90^\circ) = 5k$ . The net double kink nucleation rate is  $J = D_p C_0(x^*)/2x'$ , with  $x' = kT/\sigma bh$  and the dislocation velocity  $V = 2h(J\nu_k)^{1/2}$  if the dislocation segment length is larger than the kink mean free path  $\lambda$ . Then  $V$  depends exponentially on  $Q = F_k + W_m$ . Other theories have assumed a kink velocity limited by obstacles such as antiphase defects or point defects [4–6]. Theoretical values of  $W_m$ ,  $F_k$  exist [7,8]; experimental work is summarized in [9].

Our float-zone (FZ), P-doped Si samples were prepared by two-stage compression along  $[213]$  with final rapid cooling from  $420^\circ\text{C}$  under high stress [10]. Different mobilities leave the  $30^\circ$  and  $90^\circ$  partials on  $(1\bar{1}1)$  separated by a ribbon of stacking fault (SF) of nonequilibrium width  $d$ . The shear stress  $\sigma$  in the direction of the partial Burgers vector  $b$  can then be determined if  $d$  is known using  $\sigma = (\gamma - A/d)/b$ , where the stacking fault energy  $\gamma = 0.058\text{ J m}^{-2}$  for Si and  $A = 3.36 \times 10^{-10}\text{ N/m}$ . The force perpendicular to the line is then  $\sigma b$  per unit length. Our experiments consisted of (A) TEM video recordings at  $600^\circ\text{C}$  and  $0.3\text{ nm}$  spatial resolution of the

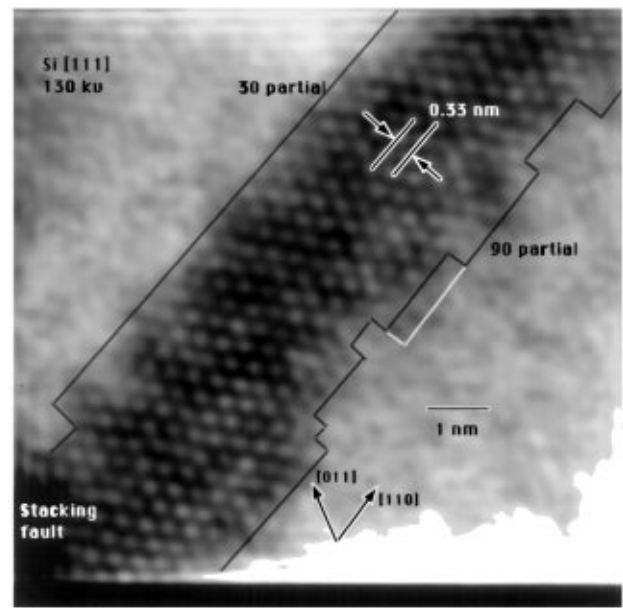


FIG. 3. TEM image of dissociated  $60^\circ$  dislocation in silicon after relaxation. Diagonal band of regular dots are six-membered rings in the stacking fault layer separating  $30^\circ$  and  $90^\circ$  partial dislocation lines. Black lines run along cores of the two partial dislocations. Fine white line shows typical alternative boundary used to estimate error in counting kinks.

relaxation process whereby the partials move under known stress from their quenched to equilibrium positions. These experiments are affected by radiation enhanced dislocation glide (REDG [11]) due to beam-induced electron-hole recombination at kinks, but are less affected by atomic-scale roughness on surfaces since successive video images (in which only kinks move) were subtracted. (B) Low-dose still images (film and image plates) of SF and partials before and after heating (with the electron beam off) to  $130^\circ\text{C}$  for relaxation. Video images were used to measure kink velocities and observe pinning; still images gave estimates of kink separations, yielding  $F_k$  using Eqs. (1) and (2).

Figure 1(b) shows the imaging conditions used [12]. The  $130\text{ kV}$  TEM electron beam runs normal to the ribbon of  $(1\bar{1}1)$  SF separating the  $90^\circ$  and  $30^\circ$  partial dislocations [Fig. 1(b)]. The SF plane generates six  $\langle 42\bar{2} \rangle/3$  Bragg beams within the SF ribbon and not elsewhere, and only these are used to form the images. These beams are forbidden by symmetry in the three-dimensional (unfaulted) diamond structure. The  $d$  spacing for the planes is  $d_{422} = h = 0.33\text{ nm}$ , or one Peierls valley wide. These valleys run along the  $\langle 011 \rangle$  tunnels in the diamond structure, orthogonal to  $\langle 42\bar{2} \rangle/3$ . Electron microdiffraction patterns show these strong “forbidden” beams [12]. Unlike small surface islands, the extended translational symmetry of the SF fault plane generates sharp reflections. As a monatomic surface island grows, diffuse elastic scattering concentrates into peaks around the forbidden reflection positions, which are absent for a thin slab of  $3n$  double

layers not containing a SF. Computed dynamical diffraction patterns from SFs have been published for varying degrees of surface roughness, together with simulated TEM images of kinks [13]. Video rate images of several  $60^\circ$  dislocation segments dissociated into  $30^\circ$  and  $90^\circ$  partials were recorded at  $600^\circ\text{C}$ . Consistent with the earlier finding that  $90^\circ$  partials are more mobile than  $30^\circ$  partials [9], motion (on the atomic scale) was confined to the  $90^\circ$  partial and still images consistently showed a higher kink density on the  $90^\circ$  partial than on the  $30^\circ$  partial. (Mobility also depends on which partial is leading [9].) Correlated kink nucleation on both partials was not observed. Figure 2(a) shows the difference between video frames recorded before and after motion of a  $90^\circ/30^\circ$  dislocation at  $600 \pm 10^\circ\text{C}$ . The SF is narrowing toward equilibrium by motion of the  $90^\circ$  partial alone. Cross correlation between stationary regions was used to align successive frames. The dark region is a thin strip of SF on the  $90^\circ$  partial, whose width measured normal to the dislocation line is three Peierls valleys ( $3d_{422} = 0.99\text{ nm}$ ). This strip has been eliminated by the passage of several kinks moving parallel to  $V_k$  as shown in Fig. 1(a). The kinks encounter obstacles at  $K$  and  $K'$ . Figure 2(b) shows the collapse of a segment of SF whose width is one Peierls valley ( $0.33\text{ nm}$ ) wide. A study of individual frames shows that the motion spans several 33 ms frames, so that upper and lower limits on the kink transit time can be made with an error of one frame. A typical single-width segment  $L = 11.7\text{ nm}$  long gave a velocity of  $205 \pm 111\text{ nm/sec}$  at  $600^\circ\text{C}$ . The stress  $\sigma = 108.5 \pm 7.5\text{ MPa}$  was obtained from the total SF width of  $9.95 \pm 0.5\text{ nm}$ . From the waiting times  $\tau = \nu_D^{-1} \exp(E_u/kT)$  at obstacles, unpinning energies  $E_u$  may also be obtained—the average of two single-width cases gave  $E_u = 2.4 \pm 0.04\text{ eV}$ . Applying the obstacle theory of kink motion [4–6] we obtain a velocity  $v_k' = L\nu_D \exp(-E_u/kT) = 2.4\text{ nm/sec}$  for the average velocity of kinks encountering many obstacles. A comparison with the instantaneous kink velocity of  $205\text{ nm/sec}$  shows that the transit time is short compared with the waiting time, as assumed in obstacle theories. Several experimentally indistinguishable mechanisms may be responsible—in particular, we cannot distinguish single kink unpinning at one end of the segment  $K$  from homogeneous double kink nucleation at midsegment followed by outward propagation to obstacles  $K, K'$  at the ends of the segment. Since extended defects are not seen at cores in still images at atomic resolution, the obstacles are likely to be dragging points which move forward with the line. We now consider their origin.

During the  $800^\circ\text{C}$  first stage of deformation, dislocations getter the P ( $2 \times 10^{13}\text{ cm}^{-3}$ ), O ( $< 10^{16}$ ), and C ( $< 10^{16}$ ) impurities in our FZ sample. Carbon is known to be ineffective in dislocation pinning [14] and vacancies and interstitials have much larger values of  $L$ , as does P (although strongly pinning) due to its low diffusion rate [15]. We find no evidence (at  $0.27\text{ nm}$  resolution) for the O or P complexes previously proposed as pinning centers

[16,17]. The impurity with highest concentration is oxygen, whose pinning effect has been studied extensively by x-ray topography in samples with controlled concentrations [18], suggesting  $L = 14.0\text{ nm}$  and an unpinning energy of about  $3\text{ eV}$  at high temperature. Electronic structure cluster calculations for likely structures suggest [19] that a single oxygen atom on the most stretched bond around the antiphase defect (soliton) can explain this result. The concentration and unpinning energy (release rate) of this defect are in rough agreement with our observations; however, beam-induced pinning effects must be considered. Previous work [20–22] suggests that the beam has two effects: the introduction of strong pinning centers at energies above the threshold for ballistic knock-on damage ( $\sim 140\text{ kV}$ ) and the enhanced diffusion of kinks (REDG) and impurities by beam-induced electron-hole pair recombination [23]. The first effect was minimized by reducing the beam energy until, at  $130\text{ kV}$  (where all this work was done), the concentration of resolvable beam-induced defects was found to be negligible. The second effect depends on the intensity and exposure time. The spacing of our obstacles is consistent with the “garland” and “cusp” features seen on  $90^\circ$  partials in previous work, thought to be due to recombination enhanced diffusion of impurities from thin foil surfaces to dislocations [24], not seen in unirradiated samples. Impurities may create a soliton-antisoliton pair at a reconstructed core which may then nucleate oxide precipitates [25]. In summary, we speculate that our  $2.4\text{ eV}$  unpinning energy is due to oxygen at antiphase defects, affected in some way by irradiation.

Still images were also recorded on video and film of a  $30^\circ/90^\circ$  dislocation under low-dose conditions (to avoid the introduction of pinning centers), both before and after annealing (with the beam off) at  $130^\circ\text{C}$  (below the kink nucleation temperature) for 15 min. Figure 3 shows a typical image, in which the partials have moved apart toward their equilibrium separation of  $5.8\text{ nm}$ . (Unlike  $90^\circ/30^\circ$  dislocations and screws, the  $30^\circ/90^\circ$  contracts during the initial deformation due to lattice friction [9].) Image calculations [12] show that the bright diagonal band of regularly spaced dots is a lattice image of the double layer of atoms which form the stacking fault plane. Pairs of atoms appear as a single dark spot, bright spots are centered on the six-fold rings of a single double layer. The borders of this band of regular dots form the partial dislocation cores, as shown. The white scale lines indicate one Peierls valley,  $0.33\text{ nm}$  wide, and the average stacking fault width corresponds to a stress on the partials of  $275\text{ MPa}$ . Although the accurate determination of kink density is complicated by the effects of surface roughness, the higher density on one partial (seen also in larger fields of view [26,27] and in many different cases) suggests that surface effects are not dominant. In addition, monatomic surface islands are not seen outside the stacking fault—these would produce similar (but lower) contrast to the stacking fault. Kinks smaller than

the critical separation  $x^* = 0.81$  nm are evidently due to surface roughness. Figure 3 shows how the error in kink density was estimated. Since  $V = 2hcv_k$ , these images may be used to estimate  $W_m$  from the kink density  $c$  and distance  $\Delta s$  the partial dislocation moves, using  $\Delta s = 2ch\Delta y$ , where  $\Delta y$  is the mean distance a kink moves in time  $\Delta t$ . Using  $\Delta y/\Delta t = v_k$  in Eq. (3) yields  $W_m = 1.24 \pm 0.07$  eV ( $U_m = 1.55$  eV).

The kink formation energy  $F_k$  may be estimated by measuring the distribution of kink-pair separations in unrelaxed images (see [1] for details). Table I shows the distribution of kink-pair separations. From this,  $c(x)$  (dimensions  $L^{-2}$ ), the unconstrained number of kink pairs with separation between  $x$  and  $x + dx$  per unit length of dislocation may be obtained. The critical separation at the saddle point is  $x^* = (\mu bh/8\pi\sigma)^{1/2} = 0.81$  nm. Extrapolation from Table I gives  $c(x^*) = 8.9 \times 10^7$  m $^{-2}$ , which, from Zeldovich [28] is half the constrained value  $c_0(x^*)$ . Using Eq. (1) with  $a = 0.384$  nm,  $T = 420$  °C gives  $F(x^*) = 1.455$  eV, so that, from Eq. (2),  $F_k = 0.5[F(x^*) + (\mu\sigma b^3 h^3/2\pi)^{1/2}] = 0.727 \pm 0.15$  eV ( $U_k = 0.74$  eV). This may refer either to a reconstructed kink or to a kink associated with a soliton [29].

Measurements on the 30° partial give approximately one-third the kink density of the 90°. Thus we find  $F_k(30) = 0.797 \pm 0.15$  eV. Our value of  $W_m = 1.24$  eV may be compared with recent *ab initio* local density approximation calculations, which give 1.8 eV [30], and is consistent with recent *ab initio* calculations [31] favoring reconstruction of the 90° core, which clears the band gap of deep states. Our value is consistent with values of 1.0–1.2 eV measured previously [20,24]. Our finding that  $F_k = 0.727$  eV may be compared with measurements by other methods which fall in the range 0.4 to 1.1 eV [7,32], and with calculations giving 0.1 eV [30], based on a hydrogen terminated cluster for the smallest kink pair, with elastic interactions dominating. (These authors comment that their method may underestimate  $F_k$ .) For segments much longer than the kink mean free path we thus obtain  $Q = F_k + W_m = 0.727 + 1.24 = 1.97 \pm 0.2$  eV. Since  $F_k < W_m$ , we find that, unlike metals, kink mobility rather than formation is the rate-limiting step controlling the motion of free dislocations in silicon. Since we cannot demonstrate the absence of widely spaced or unresolvable obstacles in unirradiated material, this work cannot distinguish the obstacle [4] and secondary Peierls-valley [1] theories of kink motion. In irradiated material, unpinning of kinks at obstacles is di-

TABLE I. The measured number of kink pairs  $N$  with separations  $x = ma$  ( $m$  integer,  $a = 0.384$  nm core period) for a 90° partial dislocation in silicon.

$N$	$m$	$x$ (nm)
3	4	1.5
2	5	1.9
2	6	2.3

rectly observed for the first time, yielding the parameters of the obstacle theory.

Work supported by NSF DMR9526100.

\*Electronic address: SPENCE@ASU.EDU

- [1] J.P. Hirth and J. Lothe, *Theory of Dislocations* (Wiley, New York, 1982).
- [2] A. Seeger and P. Schiller, *Acta Metall.* **10**, 348 (1962).
- [3] S. Marklund, *Solid State Commun.* **54**, 555 (1985).
- [4] V. Celli, M. Kabler, T. Ninomiya, and R. Thomson, *Phys. Rev.* **131**, 58 (1963).
- [5] H. J. Moller, *Acta Metall.* **26**, 963 (1978).
- [6] V. Rybin and A. Orlov, *Sov. Phys. Solid State* **11**, 2635 (1970).
- [7] H. Gottschalk, N. Hiller, S. Sauerland, P. Specht, and H. Alexander, *Phys. Status Solidi (a)* **138**, 547 (1993).
- [8] Y. Huang, J. Spence, and O. Sankey, *Phys. Rev. Lett.* **74**, 3392 (1995).
- [9] H. Alexander and H. Teichler, in *Electronic Structure and Properties of Semiconductors*, edited by W. Schroter (VCH, Weinheim, 1991).
- [10] K. Wessel and H. Alexander, *Philos. Mag.* **35**, 1523 (1977).
- [11] K. Kusters and H. Alexander, *Physica (Amsterdam)* **116B**, 594 (1983).
- [12] H. Alexander, J. Spence, D. Shindo, and N. Long, *Philos. Mag. A* **53**, 627–643 (1986).
- [13] J. C. H. Spence in *Proceedings of the 39th Annual Meeting of the Electron Microscopy Society of America*, edited by G. Bailey (Claitors, Baton Rouge, 1981), p. 120.
- [14] K. J. Sumino, *Phys. (Paris), Colloq.* **44**, C4-195 (1983).
- [15] K. Sumino and M. Imai, *Philos. Mag. A* **47**, 753 (1983).
- [16] K. Sumino, *Inst. Phys. Conf. Ser.* **104**, 245 (1989).
- [17] K. Sumino, *Mater. Res. Soc. Symp. Proc.* **14**, 307 (1983).
- [18] M. Sato and K. Sumino, *Dislocations* (University of Tokyo Press, Tokyo, 1985), p. 391.
- [19] A. Umerski and R. Jones, *Philos. Mag. A* **67**, 905 (1993).
- [20] P. B. Hirsch, A. Ourmazd, and P. Pirouz, *Inst. Phys. Conf. Ser.* **60**, 29–34 (1981).
- [21] A. Louchet, *Philos. Mag.* **43**, 1289 (1981).
- [22] H. Gottschalk, in *Electron Microscopy and Analysis 1982* (Institute of Physics, Bristol, 1982), Vol. 2, pp. 527, 528.
- [23] N. Maeda and S. Takeuchi, *Inst. Phys. Conf. Ser.* **104**, 303 (1989).
- [24] H. Gottschalk, H. Alexander, and V. Dietz, *Inst. Phys. Conf. Ser.* **87**, 339 (1987).
- [25] M. Heggie, R. Jones, and A. Umerski, *Phys. Status Solidi (a)* **138**, 383 (1993).
- [26] J. Spence, H. Kolar, and H. Alexander, *Mater. Res. Soc. Symp. Proc.* (to be published).
- [27] H. Alexander, J. Spence, D. Shindo, H. Gottschalk, and N. Long, *Philos. Mag.* **53**, 627 (1986).
- [28] J. B. Zeldovich, *Acta Physicochem. USSR* **18**, 1 (1943).
- [29] V. V. Bulatov, S. Yip, and A. S. Argon, *Philos. Mag. A* **72**, 453–496 (1995).
- [30] S. Oberg, P. Sitch, R. Jones, and M. Heggie, *Phys. Rev. B* **51**, 13 138 (1995).
- [31] J. Bigger, D. McInnes, A. Sutton, M. Payne, I. Stich, R. King-Smith, D. Bird, and L. Clarke, *Phys. Rev. Lett.* **69**, 2224 (1992).
- [32] R. Hull and J. Bean, *Phys. Status Solidi A* **138**, 533 (1993).